HHS Public Access

Author manuscript

Cancer Res. Author manuscript; available in PMC 2017 January 15.

Published in final edited form as:

Cancer Res. 2016 January 15; 76(2): 429–439. doi:10.1158/0008-5472.CAN-15-1576.

Redirecting transport of nanoparticle albumin-bound paclitaxel to macrophages enhances therapeutic efficacy against liver metastases

Tomonori Tanei, **Fransisca Leonard**, **Xuewu Liu**, **Jenolyn F. Alexander**, **Yuki Saito**, **Mauro Ferrari**, **Biana Godin**[1], and **Kenji Yokoi**[1]

Houston Methodist Research Institute, Department of Nanomedicine, Houston, TX

Abstract

Current treatments for liver metastases arising from primary breast and lung cancers are minimally effective. One reason for this unfavorable outcome is that liver metastases are poorly vascularized, limiting the ability to deliver therapeutics from the systemic circulation to lesions. Seeking to enhance transport of agents into the tumor microenvironment, we designed a system in which nanoparticle albumin-bound paclitaxel (nAb-PTX) is loaded into a nanoporous solid multistage nanovector (MSV) to enable the passage of the drug through the tumor vessel wall and enhance its interaction with liver macrophages. MSV enablement increased nAb-PTX efficacy and survival in mouse models of breast and lung liver metastasis. MSV-nAb-PTX also augmented the accumulation of PTX and MSV in the liver, specifically in macrophages, whereas PTX levels in the blood were unchanged after administering MSV-nAb-PTX or nAb-PTX. In vitro studies demonstrated that macrophages treated with MSV-nAb-PTX remained viable and were able to internalize, retain, and release significantly higher quantities of PTX compared to treatment with nAb-PTX. The cytotoxic potency of the released PTX was also confirmed in tumor cells cultured with the supernatants of macrophage treated with MSV-nAB-PTX. Collectively, our findings showed how redirecting nAb-PTX to liver macrophages within the tumor microenvironment can elicit a greater therapeutic response in patients with metastatic liver cancer, without increasing systemic side-effects.

Keywords

Multi-Stage nanovector; Liver metastasis; breast cancer; lung cancer; nanoparticle albumin-bound paclitaxel

[1]These authors are corresponding authors and share senior authorship: Biana Godin (BGodin@houstonmethodist.org) and Kenji Yokoi (KYokoi@houstonmethodist.org).

Disclosure of Potential Conflicts of Interest:

M. Ferrari is the founding scientist and a member of the Board of Directors of NanoMedical Systems, and a member of Board of Directors of Arrowhead Research Corporation, and hereby discloses potential financial interests in the companies. Xuewu Liu has ownership interest (including patents) in Leonardo Biosystems Inc. No potential conflicts of interest were disclosed by the other authors.

INTRODUCTION

Despite improvements in diagnosis, surgical techniques, general patient care and systemic therapies, most deaths from cancer result from the progressive growth of distant metastases. The liver is one of the dominant metastatic sites for primary gastrointestinal, breast and lung cancers. Current approaches to treat liver metastasis include hepatic resection (surgery), transcatheter arterial embolization (TAE), systemic chemotherapies, molecular targeted therapies, immunotherapies and various combinations (1). Unfortunately, patients usually do not respond sufficiently to these therapies or develop resistance, limiting 5-year survival rate to ~22% (2-4).

Transport of therapeutics from systemic circulation to the tumor cells substantially affects their efficacy (5,6). Nevertheless, poor transport and tumor uptake have been often neglected as mechanisms of drug resistance in cancer therapy. Major roadblocks for drug transport consist of biophysical barriers, such as tumor-associated blood flow, vascular permeability, and tumor stroma. Majority of liver metastases are hypovascular in comparison with surrounding uninvolved liver. Tumor lesions in the liver frequently appear either hypoattenuating or isoattenuating on clinical CT scans (7-9). In our previous study, vascular permeability in the liver metastases was decreased with respect to primary tumor (10). Thus, systemically injected contrast agent or therapeutics may not be able to accumulate sufficiently in the lesion.

On the other hand, any substance administered intravenously (i.v.) rapidly encounters the phagocytic cells of the livercalled Kupffer cells (KC). These tissue associated hepatic macrophages represent ~ 10-20% of all the cells in the healthy liver (11), and higher numbers are present in the close proximity of metastatic loci due to the recruitment of monocytes/macrophages from bone marrow in response to tumor-associated inflammation (12). The pronounced presence of these phagocytic cells in the proximity of the liver lesions has been utilized in the clinic for imaging liver tumors with i.v. injection of super paramagnetic iron oxide nanoparticles (SPION) (13). Solid SPION particles are intrinsically taken up by the liver macrophages thus enhancing the T2 contrast around the lesion.

To overcome multiple successive biophysical barriers and carry therapeutics to the tumor microenvironment more efficiently, we have developed multi-stage nanovector (MSV) deliverysystems composed of mesoporous silicon particles (14-16). MSV systems are comprised of several nanocomponents, or stages, which can be designed based on the desired functionality (17,18). First stage porous silicon particles can target various cell populations, such as tumor-associated endothelial cells or macrophages (18-21). The nanopores of the first stage vector are loaded with the second stage therapeutic agent/ nanoparticles. When MSV associates with the target cells in the tumor microenvironment, the second-stage therapeutic nanoparticles/macromolecules are released into the tumor lesion by time-dependent degradation of the silicon carrier. Several studies by our group have reported an increased efficiency when MSV approach was utilized for the therapy of various primary tumors (22-24).

Nanoparticle albumin-bound paclitaxel (nAb-PTX) is a clinically used nanoformulation of paclitaxel designed to overcome the toxicities associated with the Cremophor® based formulation of PTX. nAb-PTX is currently approved for the therapy of advanced breast, lung and pancreatic tumors. This albumin-bound therapeutic targets an albumin transporter expressed on vascular endothelial cells (25), thereby, activating transport across the tumor vessel wall and allowing PTX to accumulate in the tumor. Although nAb-PTX has shown better therapeutic efficacy than PTX, its clinical efficiency in the case of tumor mass in the liver lesions is marginal (26).

In this study, we aimed at evaluating the therapeutic efficacy of redirecting nAb-PTX from tumor vessels to the macrophages in the proximity of the metastatic tumors in the liver by means of MSV carrier. MSV-nAb-PTX was designed and characterized *in vitro* and *in vivo* studies. *In vivo* studies in experimental liver metastasis of breast and lung tumormodels show that the proposed approach significantly enhanced therapeutic transport to the liver and extended the survival of animals as compared to the clinically used nAb-PTX.

MATERIALS AND METHODS

Fabrication, characterization of MSV and loading of nAb-PTX

Discoidal MSV with 1μm× 0.4μm (d×h) were fabricated in a microelectronics facility via photolithography and electrochemical etching as previously described(19) (see also Supplementary Information, SI). The particles were modified with 3-aminopropyl-triethoxysilane (APTES) (19,21,27) and lyophilized using Freezone Freeze Dry System (Labconco, Kansas City, MO). nAb-PTX (Abraxane®, Celgene, Summit, NJ) particles injectable suspension was loaded to lyophilized MSV in aliquots, followed by drying under low pressure system (28). MSV were fluorescently labeled with DyLight 650 (AbCam, USA) when required (29). Release of FITC-albumin from the MSV was tested in two pHs: 4.5 and 7.4 (for cell organelles and plasma/buffer) at 37°C and 100 rpm for 1-96 hours. 1N NaOH solution (10%v/v per sample) was added to all samples prior to the measurements to avoid the loss of fluorescence of FITC-albumin in acidic pH. The standard curves were plotted based on the FITC-albumin solutions treated in the same manner (See SI).

Cell culture

The 4T1 murine breast cancer cells and 3LL murine lung cancer cells were obtained from ATCC (Manassas, VA) and used within 20 passages. The cells were cultured in Minimum Essential Medium (MEM) supplemented with 10% FBS, 1% penicillin-streptomycin,1% GlutaMAX, 1% NEAA,1% MEM Vitamin, 1% sodium pyruvate at 37°C in a humidified atmosphere with 5% CO2.

Isolation of mouse abdominal macrophages

Brewer thioglycollate (3mL, Becton-Dickinson, NJ, USA) were injected into mice peritoneum 72 hours prior to cell harvest. The peritoneal cavity was then injected with 5 mL PBS containing 3mM EDTA, and the fluid was collected and centrifuged to obtain macrophages. The cells were seeded at approximately 10^6 cells/well in 6 well plates with MEM and supplements as listed above.

Models of breast and lung cancer liver metastasis and primary breast tumor

Female Balb/C and C57BL/6 mice, 6-8 weeks old, were purchased from Charles River Laboratories (Wilmington, MA). The mice were maintained in animal facilities at Houston Methodist Research Institute approved by the American Association for Accreditation of Laboratory Animal Care and in accordance with current regulations and standards of the United States Department of Agriculture, Department of Health and Human Services, and National Institutes of Health.

To establish experimental liver metastasis, breast cancer 4T1 cells (1×10^5 / 100μL) or lung cancer 3LL cells (3×10^5 cells/ 100μL) were injected into the spleen of female Balb/C or C57BL/6 mice, respectively (10). The cells injected in the spleen disseminate to the liver through portal vein, producing experimental liver metastasis (30). To evaluate therapeutic efficacy and survival of the tumor-bearing mice described, the spleen was resected 10 minutes after the injection of the tumor cells to prevent growth of primary tumor in the spleen. For determination of MSV tissue distribution, the spleen was not resected. 4T1 cells were injected into the mammary fat pad of Balb/C mice to establish orthotopic murine breast cancer.

All the surgical procedures are approved by the Institutional Animal Care and Use Committee (IACUC) of Houston Methodist Research Institute under the protocol AUP-0514-0032.

Intravital microscopyanalysis

Alexa Fluor 488 40 kDa (green) and Alexa Fluor 538 3 kDa (red) dextrans (Molecular Probes, Oregon, USA) were injected intravenously into the retro-orbital space of the mice immediately before Intravital Microscopy (IVM) recording for visualization of blood flow dynamics (31). Mice were anesthetized with isoflurane and mounted on heated microscope stage during IVM imaging under Nikon A1R multi-photon microscope (Nikon Inc., Melville, NY). The liver was exposed by a midline incision through the abdominal wall. The fluorescent images of the tumors and unaffected (control) liver (n=12-15) were recorded 0-60 min after the injection of the tracers. The images were processed for evaluation of fluorescent intensities of the tracers inside and outside the lesions at different times using NIS-Elements Image Processing software (Nikon, USA). The recorded fluorescent intensities in the site of interest (in arbitrary units) were then normalized to the fluorescent intensity in the unaffected liver.

Evaluation of therapeutic efficacy and survival

Seven days after the injection of tumor cells, the mice (n=5-8) were randomized into three treatment groups: (A) untreated control (PBS); (B) nAb-PTX (75 mg/kg nAb-PTX, equivalent to 7.5 mg/kg PTX); and (C) MSV-nAb-PTX (75 mg/kg nAb-PTX). The therapy was administered three times via i.v. injections at five days interval. 24 hours after the last treatment, the mice were sacrificed, and the livers were excised and weighed. Livers were either fixed in 4% formalin or embedded in OCT compound for histological and immunohistochemical analysis. Diameter of liver metastases was assessed by light microscopy analysis of histology slides.

In survival experiments, 4T1 or 3LL liver metastases bearing mice were continuously treated with the above regiments once in every five days (n=10) until the mice became moribund and were sacrificed.

Immunostaining with Ki67, F4/80 antibody and TUNEL system

Formalin embedded tissues were sectioned and stained with Hematoxylin and Eosin (H&E). Frozen sections were fixed with 4% paraformaldehyde in PBS for 15 min. For staining of proliferating cells, or macrophage , the sections were incubated with anti-mouse Ki67 rabbit polyclonal antibody (Abcam, Cambridge, MA), anti-mouse F4/80 or CD68 rat polyclonal antibody (AbD serotec, Raleigh, NC) at 4°C overnight followed by incubation with corresponding secondary antibody, respectively. TUNEL assay was performed using TUNEL System (Promega Biosciences, LLC, San Luis Obispo, CA USA) according to the manufacturer's protocol. The sections were imaged under laser scanning confocal microscope (Nikon Inc.), and the images were analyzed using NIS Elements software. DAPI nuclear stain was used to define the number of cells and the border of the tumor lesions (based on the density of nuclei). Fluorescent images (n=10-12) were captured and processed for regions of interest (ROI) using NIS elements software. To evaluate the macrophage distribution in various regions of the liver, the relative fluorescent intensities of F4/80 cells in ROI inside the tumor, tumor periphery (40-50 μm from the tumor border) and in the unaffected tissue were measured and normalized to DAPI signals (number of cells).

MSV tissue distribution

MSV biodistribution was assessed as previously described (19,32). Briefly, silicon (Si) levels were quantitatively measured in the liver and major organs using inductively coupled plasma atomic emission spectrometry (ICP-AES). Tissue extracts were processed for ICP analysis spiked with Yttrium as an internal standard and analyzed for Si contents (250.69 nm, 251.43 nm, 251.61 nm and 288.158 nm). An aliquot of the MSV suspension injected was dissolved in 0.1 N NaOH overnight and tested by ICP to assess the injected dose of Si. Silicon levels were calculated as micrograms of silicon per grams of tissue and further normalized to the injected dose to obtain % of injected dose. For evaluation of MSV distribution in the liver tissue, 4T1 tumor in the liver bearing Balb/C mice were injected intravenously with fluorescent MSV. The mice were sacrificed 24 hours post-injection and the livers were excised, embedded in OCT and sectioned.

Cell proliferation assay *in vitro*

MTT (Sigma, USA) and WST1 (Clonetech, CA, USA) assays were performed according to the manufacturer's protocols to access viability of 4T1/ 3LL cells and abdominal macrophages, respectively. Cancer cells and abdominal macrophages were seeded into 96-well tissue culture plates at concentrations 1×10^3 cells/well and 1×10^4 cells/well, respectively, and incubated with increasing concentrations of nAb-PTX and MSV-nAb-PTX for 72 h. Cell viability was assessed at 570 nm and 440 nm for MTT and WST-1 assays.

Sample preparation for quantification of PTX by LC/MS

Amount of PTX internalized and released by macrophages was determined *in vitro* (See SI). In brief, macrophages were incubated with MSV, nAb-PTX or MSV-nAb-PTX for 1 and 2 days and the cells were lysed for analysis of PTX internalization. Additionally, the macrophages were incubated with MSV, nAb-PTX or MSV-nAb-PTX, washed and further cultured with fresh medium. After 1 and 2 days, the supernatant was measured for the amount of PTX released. The amount of PTX in the plasma and liver of mice injected with PBS, MSV, nAb-PTX, and MSV-nAb-PTX was also determined after 1 and 3 days of treatment and measured by liquid chromatography-tandem mass spectrometry (LC-MS/MS) analysis (see SI).

To evaluate cytotoxic activity of PTX released from macrophages, conditioned medium was added to cancer cells and cell death was evaluated by MTT assay after 3 days.

Statistical analysis

All quantitative parameters are presented as a mean with standard deviation. Statistical analysis was performed by the Mann–Whitney U test for unpaired samples, and survival analysis was done by the Kaplan-Meier method and compared by the Log rank test using the SPSS software. P value of < 0.05 is accepted as indicative of a significant difference.

RESULTS

Transport of macromolecules into the tumor lesions in the liver

Clinically, liver lesions frequently appear hypoattenuated, pointing towards the low perfusion, extravasation and diffusion of the contrast reagents in the tumors as compared to the uninvolved organ. To confirm that our animal models of liver metastasis are characterized by similar features, we have performed IVM imaging of i.v. injected 3 kDa and 40 kDa dextrans in the liver lesions. Figure 1 (A and B) shows that the transport of both molecules into the loci of liver metastasis was significantly impaired. Quantitatively (Figure 1B), the intensity of 3 kDa probe in the lesion ranged from 35-70% of that of the unaffected tissue, while for 40 kDa dextran the concentration in the unaffected tissue was 4 times higher than inside the lesion. nAb-PTX is an albumin-bound drug and albumin has a similar hydrodynamic diameter as the high molecular weight dextran (~10 nm). We have also confirmed that similarly to the clinical findings (33), both models show increased number of macrophages in the proximity of the tumor lesions in the liver (Fig. 1C). The concentration of macrophages on the periphery of the tumor lesions in the liver was twice higher than in the uninvolved organ (39.8 vs. 21.7%, $P<0.01$, respectively).

Design and characterization of MSV-nAb-PTX

Since we have previously shown that MSV particles have high affinity to macrophages *in vitro* and *in vivo* (18,19,21), we have further designed the MSV-nAb-PTX carrier to shift the intrinsic transport characteristics from albumin transporters involved in nAb-PTX and located on the blood vessels towards association with macrophages in the proximity of the lesions in the secondary liver tumors. The pores of MSV carrier were loaded with nAb-PTX and FITC-albumin as a model fluorescent molecule with the same physico-chemical

characteristics and the release profiles in aqueous media of two different pHs (7.4 and 4.5) were assessed by fluorimetry. The two pHs were chosen to represent the physiologic pH of the injection solution and the plasma and the acidic pH of cell endosomes. MSV were efficiently loaded with FITC-albumin and nAb-PTX (Figure 2). Zeta potential (ζ) of MSV was affected by the loading. APTES-MSV are positively charged due to primary amines and ζ changes due to the loading of albumin-bound drug/probe since albumin has a net negative charge in the neutral environment. FITC-albumin loading efficiency was in the range of 80-94%, and the MSV were uniformly loaded with the macromolecule as can be seen from the confocal micrographs. It is known that nAb-PTX in the powder have particle diameter of 130nm (34). However, when immersed into aqueous solution, it disintegrates into albumin aggregates that have a hydrodynamic diameter of 12.4 nm (SI Figure 1), comparable to the hydrodynamic diameter of the albumin. Thus, the particles can be efficiently loaded into the pores of MSV with diameters ranging from 20 to 50nm. The optimized loading efficiency of nAb-PTX was 64%, which depended on the method of loading, with the most efficient one being vacuum assisted loading (as described in Materials and Methods section).

In terms of release, albumin was more prompt to be released in the normal pH and was not released from the MSV in acidic environment (Figure 2C). This points towards the ability of MSV to protect the drug in the endosomal compartment. Our previous studies have shown that MSV can be efficiently released from the macrophages and endothelial cells by exo- and trans-cytosis (35).

Biodistribution of MSV and the nAb-PTX

The organ distribution of MSV and the drug in the models of experimental liver metastasis was evaluated (Figure 3). In both mice bearing breast tumors in the liver and healthy mice, the highest concentration of MSV among the organs tested was in the liver. In the animals with liver metastasis, significantly higher concentrations of MSV in the liver was assessed as compared to the healthy mice (~36.9% vs. 23.4%, $P<0.01$). This can be related to the increased quantities of macrophages in the affected livers (Figure 1C).

Further, to assess the levels of nAb-PTX delivered intravenously in the blood plasma and livers, the mice bearing liver metastases were injected either with MSV-nAb-PTX, nAb-PTX or PBS (untreated control) (Fig. 3 B and C). One day after the administration, PTX concentration in the plasma was not significantly different for nAb-PTX vs. MSV-nAb-PTX. On the other hand, the amount of PTX accumulated in the liver was three times higher for MSV-nAb-PTX than for nAb-PTX ($P<0.05$). To confirm the localization of the MSV in the liver tissue, we have immunostained macrophages with CD68 antibody. As shown in Fig. 3D, co-localized confocal images of MSV (red) and macrophages (green) confirmed the homing of MSV into the liver macrophages.

Therapeutic efficacy: MSV-nAb-PTX vs. nAb-PTX

The mice bearing experimental liver metastasis of breast and lung tumors were treated with MSV-nAb-PTX, nAb-PTX or PBS (untreated control), three to four times once every five days. The mice were sacrificed and the livers were excised and processed for evaluation of the size/number of the lesions macroscopically and microscopically, weighted and processed

for evaluation of cancer cell apoptosis and proliferation. Macroscopically, we have confirmed the presence of numerous large tumor (light) lesions on the liver surface in the untreated control group (Supplementary Figure 2). The tumor lesions appeared smaller in the nAb-PTX group, but the least number of lesions and the smallest size were observed in the tumor bearing mice treated with MSV-nAb-PTX. Liver weight was lower in the both models treated with MSV-nAb-PTX as compared to nAb-PTX (Figure 4A, $P < 0.05$). It is noteworthy that in the healthy animals, the liver weights ranges between 0.9-1.2 grams, similarly to what was measured for liver metastasis bearing mice following the therapy with MSV-nAb-PTX.

Furthermore, Figure 4B shows MSV-nAb-PTX enabled a significant extension of survival of the tumor-bearing mice as compared to the other two therapies (nAb-PTX vs. MSV- nAb-PTX: $P<0.05$ for 4T1 and $P <0.01$ for 3LL, n=10/each group).. No changes in the number of macrophages in the unaffected liver (Figure 4C) and body weight of the animals (data not shown) were observed indicating both nAb-PTX and MSV- nAb-PTX were not toxic.

Histological evaluation consequently revealed that the tumor diameters at microscopic level in breast (4T1 cells) or lung (3LL cells) liver metastases were significantly smaller in the mice treated with MSV-nAb-PTX as compared to other therapy groups (Figure 5A, SI Fig. 3). We have further performed an immunohistochemical evaluation of the lesions. Percentages of Ki67 positive cancer cells in the lesions as a marker for the cell proliferation and TUNEL positive cells as a marker for apoptosis were imaged (Figure 5B). The number of Ki67 positive cancer cells (pink) was reduced in MSV-nAb-PTX group as compared to two other groups. The proliferation index (% proliferated cells) after MSV-nAb-PTX treatment was also significantly lower than those mice were treated with nAb-PTX ($P<0.01$ in 4T1 model, $P<0.05$ in 3LL model) (Figure 5C). On the other hand, as shown in Figure 5D, the number of TUNEL positive cancer cells (green cells) and the apoptosis index were significantly higher in MSV-nAb-PTX treated group in both models as compared to the mice treated with nAb-PTX ($P<0.05$ for both models).

Macrophages as a depot for PTX

The cytotoxicity of MSV-nAb-PTX and nAb-PTX to the cancer cells and primary abdominal murine macrophages was assessed using MTT and WST-1 assays, respectively (Supplementary Figure 4). Cancer cells were less sensitive to MSV-nAb-PTX than to nAb-PTX, pointing towards slow release of nAb-PTX from the carrier. The IC_{50} of nAb-PTX vs. MSV-nAb-PTX for inhibition of the 4T1 breast and 3LL lung cancer cells growth were in the range of 0.1 - 0.5 μg/mL. In contrast, macrophages were not sensitive to the agents and their viability was slightly affected only in the 50 μg/mL concentration range. These *in vitro* results support the *in vivo* findings that macrophages in the uninvolved liver were not affected by the therapeutics (Figure 4C).

We have then examined the capability of macrophages to serve as a depot for PTX. The amount of PTX internalized into the macrophages was examined 1 and 2 days after the incubation of abdominal macrophages with MSV-nAb-PTX or nAb-PTX *in vitro*, and determined by LC-MS/MS. The quantities of PTX accumulated in macrophages treated with MSV-nAb-PTX were significantly higher than those treated with nAb-PTX (Figure 6A).

Next, we have evaluated whether macrophages can release the internalized drug extracellularly. In this experiment, macrophages were incubated with media containing control PBS, nAb-PTX, or MSV-nAb-PTX for one or two days, then media was discarded, macrophages were washed, and fresh media without therapeutics was added to culture wells. The amount of PTX released into the culture wells 24 hours after the incubation was quantified by LS-MS/MS. Higher amount of PTX was released from macrophages into culture media when macrophages were pre-incubated with MSV-nAb-PTX as compared to nAB-PTX (Figure 6B). Interestingly, expression of p-glycoprotein, which is associated with efflux pumps for various chemotherapeutics including PTX, was increased in macrophages when incubated with MSV-nAb-PTX and nAb-PTX as compared to control media (Figure 6 C-D).

Finally, we determined PTX released from macrophages preserves the cytotoxic effect on cancer cells. The supernatants containing the drug released from the macrophages were added to the cancer cells and assessed for their effect on the tumor cell proliferation. Figures 6C and D show that the macrophage condition media following the pre-incubation with MSV-nAb-PTX were the most efficient to inhibit the growth of 4T1 (Figure 6E) and 3LL cells (Figure 6F) respectively, demonstrating that the released drug is therapeutically active.

DISCUSSION

In this study we describe a novel approach to increase the efficacy of currently used large molecular weight/nanoparticle based agents for the therapy for liver metastases of breast and lung cancer. Currently, efficient therapies for tumors metastasizing to the liver are not available and the condition is frequently considered terminal. nAb-PTX is approved by the Food and Drug Administration for therapy against advanced breast, non-small cell lung and pancreatic cancers; however, its clinical efficiency against liver lesions has not been reported. It is the first of a new class of anticancer agents that incorporate albumin-nanoparticle technology and exploit the unique properties of albumin, a natural carrier of lipophilic molecules in the mammalian serum (36). The albumin-bound nanoparticle was designed to target an albumin-specific receptor (gp60) expressed on vascular endothelial cells, thereby activating transport across the tumor vessel wall, allowing PTX to penetrate the endothelium and reach the tumor cells in higher concentration (36). Additionally, nanotherapeutics including nAb-PTX have an advantage over free chemotherapeutics because they preferentially accumulate into tumor sites utilizing Enhanced Permeation and Retention (EPR) effect on tumor (37). Thus, efficacy of nAb-PTX can be correlated with the levels of angiogenesis in the tumors. In contrast to the primary tumors, which generally possess angiogenesis and enhanced blood flow and are characterized by the pronounced EPR, secondary tumors growing in the liver are not well perfused with blood and their vascular permeability is limited as confirmed by our IVM imaging of the tumor-bearing mice (Figure 1). These findings are in agreement with the strong clinical evidence of CT imaging data of patients with secondary liver tumors, which appear less perfused when contrast agents are injected intravenously. These biophysical barriers for transport of therapeutics in the liver metastases diminish the transport advantage of nAb-PTX, thus alternative strategies to increase the therapeutic efficacy of this agent is being pursued.

To overcome the barriers and produce higher drug concentrations at the tumor site in the liver, hepatic arterial infusion (HAI) through catheter has been tested. Phase I clinical study of HAI-nAb-PTX has shown safety, clinical efficacy and higher drug concentration in the liver as compared to nAb-PTX given intravenously (38). However, the drawbacks of the HAI include the invasiveness of the procedure, need for an experienced team of surgeons, radiologists and medical oncologists as well as possible complication of implanting the catheter into the major artery (39). Our results show that by utilizing the interactions of MSV with the liver macrophages surrounding the tumor lesions, we could enhance the transport of nAb-PTX into the liver by i.v. injection of therapeutic which is more feasible, doesn't require specifically trained surgical personnel and safer as compared to HAI-nAb-PTX. Our approach is sustained by the observation that higher numbers of macrophages were found to accumulate in the close proximity of the tumor due to the recruitment of monocytes/macrophages from the bone marrow, responding to tumor-related inflammatory signals (12). It is well known that any solid particulate administered intravenously immediately encounters and internalized by the liver macrophages. On the other hand, albumin-based conjugates do not possess similar characteristics. Thus, to increase the localization of the albumin-bound PTX nanoparticle into the liver metastasis loci by enhancing its association with macrophages, we utilized multi-stage nanovector (MSV) systems composed of mesoporous silicon particles (14-16).

The MSV system is comprised of several stages: first stage, mesoporous silicon particles (S1MP), target elements in the tumor microenvironment, while the second stage nanoparticles (S2NP, e.g. nAb-PTX) encapsulated in the pores of S1MP are slowly released in the proximity of the tumor cells and affect these cells. Re-directing nAb-PTX transport from tumor vessels, which represent its original target and are not functional in the secondary liver tumors, to macrophages, which are abundant in the proximity of breast and lung liver metastasis should increase transport of therapeutics to tumors in the liver. Previous studies have shown that micrometastasis accumulate higher quantities of macrophages than more mature tumor lesions (40,41), indicating that MSV-nAb-PTX could also be beneficial to prevent the development of micrometastases into macrometastasis.

The biodistribution of MSV into the various major organs of healthy and the tumor-bearing mice after i.v. injection determined that significantly higher quantities of MSV were localized in the livers of tumor bearing mice as compared to control healthy animals-(36.9 vs. 23.4% of injected dose, respectively) (Figure 3A). This can be related to the tumor associated inflammation and recruitment of the monocytes from bone marrow to the area surrounding the liver metastasis. We found preferential accumulation of MSVs in the liver as compared to other organs (e.g. lungs) which also contain resident macrophages. The difference can be explained by the abundance of macrophages in the liver; macrophages represent approximately 10-20% of all the cells in healthy liver and 80-90% of whole tissue body macrophages (11). Liver macrophages comprise liver capillary wall along with endothelial cells. In contrast, resident macrophages in the other organs exist outside blood vessels or inside vessels with lesser extent (42,43), so injected MSVs have less of a chance to encounter macrophages in the lungs and spleen as compared to liver macrophages.

To validate macrophages serve as a depot for MSVs, we have previously tested the elimination of macrophages in the liver using clodronate liposomes (44) to reduce the accumulation of MSV in the organ. For this purpose, we used mice with primary breast 4T1 tumor grown in the mammary fat pad with the hypothesis that elimination of tissue macrophages (including liver macrophages) could significantly shift the biodistribution of MSVs towards the tumor. However, we observed clodronate liposomes induced severe and acute toxicity in tumor-bearing animals even at the lower dose of the drug. Close to 50% of the animals were unable to overcome and succumbed due to the drug administration. Thus, we concluded that in cancer-bearing sick animals, macrophages play a protective role for the overall animal health. Total elimination of the tissue macrophages can significantly jeopardize the well-being of the animals. The number of survivors was not sufficient for the statistical analysis, but the results showed a clear trend that elimination of liver macrophages increased the accumulation in the primary breast tumor (Supplementary Fig. 5). Additionally, we have performed studies in 3D tumor spheroids using a co-culture of tumor cells and macrophages. These studies show the lack of macrophages significantly hampers the therapeutic efficacy of MSV-nAb-PTX (manuscript in preparation).

We have constructed MSV-nAb-PTX by loading the S1MP nanopores with nAb-PTX and evaluated the amount of PTX in the systemic circulation and in the livers of the tumor-bearing mice using LC-MS/MS. Although the amount of PTX was significantly higher in the liver of mice treated with MSV-nAb-PTX as compared to that in the mice treated with nAb-PTX, there was no significant difference in the PTX concentration in the systemic circulation of the two groups of mice. These results indicate the potential clinical advantage using MSV-nAB-PTX to increase therapeutic efficacy for the tumors in the liver without increasing the incidence of systemic side effects. It is important to note that there was no body weight reduction in the mice treated with MSV-nAb-PTX as compared to the other groups. This is in accordance with a clinical study using HAI-nAb-PTX which has shown increased concentration of PTX in the liver without increasing peak concentration in the systemic circulation and the chance for systemic adverse events (38,39)). The three-fold higher concentration of the drug in the affected liver delivered by MSV also suggest that treatment interval can be extended for MSV-nAb-PTX as compared to nAb-PTX to possibly enable similar therapeutic benefits.

Interestingly, macrophages in the liver were not killed by the chemotherapeutic agent as confirmed by *in vivo* and *in vitro* studies. The number of macrophages in the uninvolved liver counted by immunofluorescence imaging of macrophages in the mice treated with control, nAb-PTX or MSV-nAb-PTX was unchanged (Figure 4C). Macrophages maintained their viability at high concentrations of PTX which were more than hundred times higher than those required to kill >90% of 4T1 and 3LL cells (Supplemental Figure 4). One of the reasons for resistance of macrophages to PTX can be attributed to increased expression of p-glycoprotein which is associated with efflux pumps on macrophages when incubated with PTX (Figure 6C-D). This is also an important factor in the ability of macrophages to excrete the accumulated drug to the tumor microenvironment. PTX enhances the polymerization of tubulin to stable microtubules and blocks cells in the G2/M phase of the cell cycle and such cells are unable to form a normal mitotic apparatus (45). On the other hand, macrophages

are terminally differentiated monocytes, a non-dividing cell population (46); therefore, they may not be affected by PTX.

Since, as earlier discussed, macrophages are engulfing MSV, it was important to determine whether macrophages can internalize and release the therapeutic agent from MSV *in vitro* (Figure 6). Macrophages internalized and released significantly higher quantities of PTX when the cells were cultured with MSV-nAb-PTX as compared to nAb-PTX. These results indicate advantage of using MSV as a carrier of nAb-PTX to enhance the transport of the PTX into the liver tumor microenvironment. In the next set of experiments, following the incubation of macrophages with nAb-PTX or MSV-nAb-PTX, the cells were washed and further incubated with fresh media without therapeutics. The concentration of PTX released from the cells was three times higher when the cells were pre-incubated with MSV-nAb-PTX as compared to nAb-PTX. Finally, we confirmed that the released drug from macrophages maintained its cytotoxicity to the breast and lung tumor cells *in vitro.*

To summarize the proposed mechanism of action, the efficacy of MSV-nAb-PTX as compared to nAb-PTX for the therapy of liver metastasis of breast and liver cancer can be related to redirecting the transport of nAb-PTX from tumor vessels towards the macrophages in the tumor microenvironment, which are abundant in the proximity of the lesions in the liver. We have shown that higher quantities of nAb-PTX can be transported to the liver when nAb-PTX is packed in MSV. MSV-nAb-PTX is internalized by the liver macrophages accumulating especially in the close proximity of the metastatic lesions in the liver. Macrophages can retain nAb-PTX, keep viability and release the drug, possibly through efflux pumps. The increased concentration of the therapeutic agent for the prolonged period of time in the proximity of the liver lesions governs the diffusion of the agent into the microenvironment eventually affects the viability of cancer cells nearby, inhibits tumor cell proliferation and induces apoptosis. MSV-nAb-PTX significantly enhanced therapeutic efficacy of nAb-PTX in terms of inhibition of tumor growth and extension of survival.

The therapeutic efficacy of agents in battling tumors can be hampered not only by the intrinsic molecular resistance mechanisms developed in cancer cells but also by the insufficient quantity of the therapeutics transported to cancer cells from the systemic circulation (5,6). Transport of therapeutics in the primary tumors and secondary locations significantly differs and, thus, various elements have to be considered. Understanding transport differentials in oncology, termed “transport oncophysics”, can provide a novel framework to improve cancer therapy (47). We have shown that by designing a solid particle system that will retain nAb-PTX and re-direct transport from tumor vessels to the relevant and abundant elements in the liver tumor microenvironment (macrophages), therapeutic efficacy of an agent can be significantly improved without increasing chance of developing systemic side effects. Our study provides strong rationale for clinical translation of MSV-nAb-PTX as a novel therapy for liver metastases. Relevant elements in the tumor microenvironment as a target for efficient transport of therapeutics can be different by the location of the secondary lesions (i.e, brain, lung, bone, lymph nodes, etc.). Although most of the tumors in the liver are characterized by the increased concentration of the macrophages, there are cases when macrophages are underrepresented in these tumor

lesions. In these instances, delivering the drug with MSV is not expected to provide therapeutic benefit and the deciding therapeutic modality should be rendered based on the hemodynamics in the tumors evaluated by the imaging modalities (CT/MRI with contrast reagent) (6,48). Ultimately, personalized cancer therapy should consider the transport information in the tumor lesions of the specific patient.

Supplementary Material

Refer to Web version on PubMed Central for supplementary material.

Acknowledgements

We thank David A. Engler (Houston Methodist Research Institute, Department of Proteomics) for LC-MS/MS analysis. The authors gratefully acknowledge funding from the NCI 1-U54-CA143837 and NIH 1-U54CA151668-01. M.F. and K.Y. would like to acknowledge Ernest Cockrell Jr. Presidential Distinguished Chair. We thank Ms. Hannah Kim for assistance with editorial review.

References

1. Kostov DV, Kobakov GL, Yankov DV. Prognostic factors related to surgical outcome of liver metastases of breast cancer. J Breast Cancer. 2013; 16(2):184–92. [PubMed: 23843851]
2. Selzner M, Morse MA, Vredenburgh JJ, Meyers WC, Clavien PA. Liver metastases from breast cancer: long-term survival after curative resection. Surgery. 2000; 127(4):383–9. [PubMed: 10776428]
3. Wu KL, Tsai MJ, Yang CJ, Chang WA, Hung JY, Yen CJ, et al. Liver metastasis predicts poorer prognosis in stage IV lung adenocarcinoma patients receiving first-line gefitinib. Lung Cancer. 2015
4. Gerratana L, Fanotto V, Bonotto M, Bolzonello S, Minisini AM, Fasola G, et al. Pattern of metastasis and outcome in patients with breast cancer. Clin Exp Metastasis. 2015; 32(2):125–33. [PubMed: 25630269]
5. Michor F, Liphardt J, Ferrari M, Widom J. What does physics have to do with cancer? Nature reviews Cancer. 2011; 11(9):657–70. [PubMed: 21850037]
6. Koay EJ, Truty MJ, Cristini V, Thomas RM, Chen R, Chatterjee D, et al. Transport properties of pancreatic cancer describe gemcitabine delivery and response. J Clin Invest. 2014; 124(4):1525–36. [PubMed: 24614108]
7. Pezzella F, Pastorino U, Tagliabue E, Andreola S, Sozzi G, Gasparini G, et al. Non-small-cell lung carcinoma tumor growth without morphological evidence of neo-angiogenesis. American Journal of Pathology. 1997; 151(5):1417–23. [PubMed: 9358768]
8. Stessels F, Van Den Eynden G, Van Der Auwera I, Salgado R, Van Den Heuvel E, Harris AL, et al. Breast adenocarcinoma liver metastases, in contrast to colorectal cancer liver metastases, display a non-angiogenic growth pattern that preserves the stroma and lacks hypoxia. Br J Cancer. 2004; 90(7):1429–36. [PubMed: 15054467]
9. Daly JM, Butler J, Kemeny N, Yeh SD, Ridge JA, Botet J, et al. Predicting tumor response in patients with colorectal hepatic metastases. Ann Surg. 1985; 202(3):384–93. [PubMed: 2931055]
10. Yokoi K, Tanei T, Godin B, van de Ven AL, Hanibuchi M, Matsunoki A, et al. Serum biomarkers for personalization of nanotherapeutics-based therapy in different tumor and organ microenvironments. Cancer Lett. 2014; 345(1):48–55. [PubMed: 24370567]
11. Baratta JL, Ngo A, Lopez B, Kasabwalla N, Longmuir KJ, Robertson RT. Cellular organization of normal mouse liver: a histological, quantitative immunocytochemical, and fine structural analysis. Histochem Cell Biol. 2009; 131(6):713–26. [PubMed: 19255771]
12. Heuff G, van der Ende MB, Boutkan H, Prevoo W, Bayon LG, Fleuren GJ, et al. Macrophage populations in different stages of induced hepatic metastases in rats: an immunohistochemical analysis. Scand J Immunol. 1993; 38(1):10–6. [PubMed: 8327856]

13. Reimer P, Tombach B. Hepatic MRI with SPIO: detection and characterization of focal liver lesions. Eur Radiol. 1998; 8(7):1198–204. [PubMed: 9724439]
14. Tasciotti E, Liu X, Bhavane R, Plant K, Leonard AD, Price BK, et al. Mesoporous silicon particles as a multistage delivery system for imaging and therapeutic applications. Nat Nanotechnol. 2008; 3(3):151–7. [PubMed: 18654487]
15. Sakamoto J, Annapragada A, Decuzzi P, Ferrari M. Antibiological barrier nanovector technology for cancer applications. Expert Opin Drug Deliv. 2007; 4(4):359–69. [PubMed: 17683250]
16. Serda RE, Godin B, Blanco E, Chiappini C, Ferrari M. Multi-stage delivery nano-particle systems for therapeutic applications. Biochim Biophys Acta. 2011; 1810(3):317–29. [PubMed: 20493927]
17. Godin B, Chiappini C, Srinivasan S, Alexander JF, Yokoi K, Ferrari M, et al. Discoidal Porous Silicon Particles: Fabrication and Biodistribution in Breast Cancer Bearing Mice. Adv Funct Mater. 2012; 22(20):4225–35. [PubMed: 23227000]
18. Godin B, Tasciotti E, Liu X, Serda RE, Ferrari M. Multistage nanovectors: from concept to novel imaging contrast agents and therapeutics. Acc Chem Res. 2011; 44(10):979–89. [PubMed: 21902173]
19. Godin B, Chiappini C, Srinivasan S, Alexander JF, Yokoi K, Ferrari M, et al. Discoidal Porous Silicon Particles: Fabrication and Biodistribution in Breast Cancer Bearing Mice. Adv Funct Mater. 2012; 22(20):4225–35. [PubMed: 23227000]
20. Tanaka T, Godin B, Bhavane R, Nieves-Alicea R, Gu J, Liu X, et al. In vivo evaluation of safety of nanoporous silicon carriers following single and multiple dose intravenous administrations in mice. Int J Pharm. 2010; 402(1-2):190–7. [PubMed: 20883755]
21. Yokoi K, Godin B, Oborn CJ, Alexander JF, Liu X, Fidler IJ, et al. Porous silicon nanocarriers for dual targeting tumor associated endothelial cells and macrophages in stroma of orthotopic human pancreatic cancers. Cancer Lett. 2013; 334(2):319–27. [PubMed: 23000514]
22. Tanaka T, Mangala LS, Vivas-Mejia PE, Nieves-Alicea R, Mann AP, Mora E, et al. Sustained small interfering RNA delivery by mesoporous silicon particles. Cancer Res. 2010; 70(9):3687–96. [PubMed: 20430760]
23. Shen H, Rodriguez-Aguayo C, Xu R, Gonzalez-Villasana V, Mai J, Huang Y, et al. Enhancing chemotherapy response with sustained EphA2 silencing using multistage vector delivery. Clin Cancer Res. 2013; 19(7):1806–15. [PubMed: 23386691]
24. Blanco E, Sangai T, Hsiao A, Ferrati S, Bai L, Liu X, et al. Multistage delivery of chemotherapeutic nanoparticles for breast cancer treatment. Cancer Lett. 2012; 334(2):245–52. [PubMed: 22858582]
25. Desai N, Trieu V, Yao Z, Louie L, Ci S, Yang A, et al. Increased antitumor activity, intratumor paclitaxel concentrations, and endothelial cell transport of cremophor-free, albumin-bound paclitaxel, ABI-007, compared with cremophor-based paclitaxel. Clin Cancer Res. 2006; 12(4): 1317–24. [PubMed: 16489089]
26. Blum JL, Savin MA, Edelman G, Pippen JE, Robert NJ, Geister BV, et al. Phase II study of weekly albumin-bound paclitaxel for patients with metastatic breast cancer heavily pretreated with taxanes. Clin Breast Cancer. 2007; 7(11):850–6. [PubMed: 18269774]
27. Godin B, Gu J, Serda RE, Bhavane R, Tasciotti E, Chiappini C, et al. Tailoring the degradation kinetics of mesoporous silicon structures through PEGylation. J Biomed Mater Res A. 2010; 94(4):1236–43. [PubMed: 20694990]
28. Leonard F, Margulis-Goshen K, Liu X, Srinivasan S, Magdassi S, Godin B. Low pressure mediated enhancement of nanoparticle and macromolecule loading into porous silicon structures. Mesoporous biomaterials. 2014; 1(1) 10.2478/mesbi-014-0002.
29. Tasciotti E, Godin B, Martinez JO, Chiappini C, Bhavane R, Liu X, et al. Near-infrared imaging method for the in vivo assessment of the biodistribution of nanoporous silicon particles. Mol Imaging. 2011; 10(1):56–68. [PubMed: 21303615]
30. Morikawa K, Walker SM, Jessup JM, Fidler IJ. In vivo selection of highly metastatic cells from surgical specimens of different primary human colon carcinomas implanted into nude mice. Cancer Res. 1988; 48(7):1943–8. [PubMed: 3349467]

31. van de Ven AL, Wu M, Lowengrub J, McDougall SR, Chaplain MAJ, Cristini V, et al. Integrated intravital microscopy and mathematical modeling to optimize nanotherapeutics delivery to tumors. AIP Advances. 2012; 2(1)
32. Srinivasan S, Alexander JF, Driessen WH, Leonard F, Ye H, Liu X, et al. Bacteriophage Associated Silicon Particles: Design and Characterization of a Novel Theranostic Vector with Improved Payload Carrying Potential. J Mater Chem B Mater Biol Med. 2013; 1(39)
33. Miyagawa S, Miwa S, Soeda J, Kobayashi A, Kawasaki S. Morphometric analysis of liver macrophages in patients with colorectal liver metastasis. Clin Exp Metastasis. 2002; 19(2):119–25. [PubMed: 11964075]
34. Agency EM. Nanoparticle Albumin Bound Paclitaxel Annex 1-Summary of Product Characteristics. European Medicines Agency. Apr 4.2013
35. Ferrati S, Mack A, Chiappini C, Liu X, Bean AJ, Ferrari M, et al. Intracellular trafficking of silicon particles and logic-embedded vectors. Nanoscale. 2010; 2(8):1512–20. [PubMed: 20820744]
36. Yardley DA. nab-Paclitaxel mechanisms of action and delivery. J Control Release. 2013; 170(3): 365–72. [PubMed: 23770008]
37. Maeda H, Wu J, Sawa T, Matsumura Y, Hori K. Tumor vascular permeability and the EPR effect in macromolecular therapeutics: a review. J Control Release. 2000; 65(1-2):271–84. [PubMed: 10699287]
38. Fu S, Naing A, Moulder SL, Culotta KS, Madoff DC, Ng CS, et al. Phase I trial of hepatic arterial infusion of nanoparticle albumin-bound paclitaxel: toxicity, pharmacokinetics, and activity. Mol Cancer Ther. 2011; 10(7):1300–7. [PubMed: 21571911]
39. Bertino JR. Implantable pump for long-term chemotherapy administration via the hepatic artery: has it fulfilled its promise? J Clin Oncol. 2008; 26(28):4528–9. [PubMed: 18824703]
40. Higashi N, Ishii H, Fujiwara T, Morimoto-Tomita M, Irimura T. Redistribution of fibroblasts and macrophages as micrometastases develop into established liver metastases. Clin Exp Metastasis. 2002; 19(7):631–8. [PubMed: 12498393]
41. Bugelski PJ, Kirsh RL, Sowinski JM, Poste G. Changes in the macrophage content of lung metastases at different stages in tumor growth. Am J Pathol. 1985; 118(3):419–24. [PubMed: 3976845]
42. Brain JD, Molina RM, DeCamp MM, Warner AE. Pulmonary intravascular macrophages: their contribution to the mononuclear phagocyte system in 13 species. Am J Physiol. 1999; 276(1 Pt 1):L146–54. [PubMed: 9887067]
43. Warner AE, Brain JD. Intravascular pulmonary macrophages: a novel cell removes particles from blood. Am J Physiol. 1986; 250(4 Pt 2):R728–32. [PubMed: 3963241]
44. van Rooijen N, Hendrikx E. Liposomes for specific depletion of macrophages from organs and tissues. Methods Mol Biol. 2010; 605:189–203. [PubMed: 20072882]
45. Horwitz SB. Taxol (paclitaxel): mechanisms of action. Ann Oncol. 1994; 5(Suppl 6):S3–6. [PubMed: 7865431]
46. Crofton RW, Diesselhoff-den Dulk MM, van Furth R. The origin, kinetics, and characteristics of the Kupffer cells in the normal steady state. J Exp Med. 1978; 148(1):1–17. [PubMed: 670884]
47. Ferrari M. Frontiers in cancer nanomedicine: directing mass transport through biological barriers. Trends Biotechnol. 2010; 28(4):181–8. [PubMed: 20079548]
48. Pascal J, Bearer EL, Wang Z, Koay EJ, Curley SA, Cristini V. Mechanistic patient-specific predictive correlation of tumor drug response with microenvironment and perfusion measurements. Proc Natl Acad Sci U S A. 2013; 110(35):14266–71. [PubMed: 23940372]

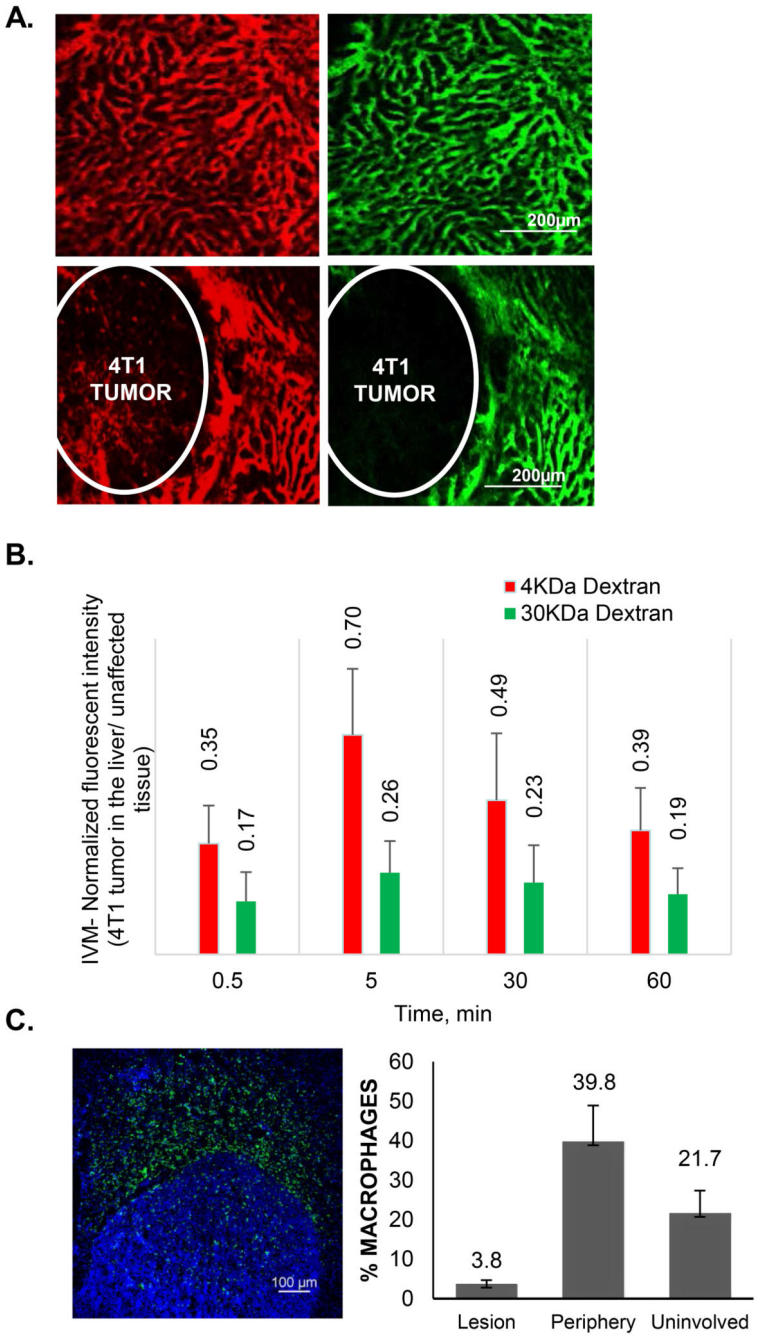

Figure 1. Transport characteristics of tumor lesions in the liver

(A) Intravital microscopic evaluation of perfusion and diffusion of 3KDa (red) and 40KDa (green) fluorescent dextrans in the normal liver (upper panels) and 4T1 liver metastasis lesions 30 minutes after the intravenous injection. (B) Quantification of fluorescent intensities of the dextrans in the lesions in the liver as normalized to the fluorescence intensity in the unaffected liver. (C) Distribution of the macrophages in the liver with tumor lesions. The macrophages are stained by F4/80 antibody (green) and the number of macrophages inside of the lesion, the periphery of the tumor (40-50 micron from the tumor

border) and in the unaffected liver is normalized to the number of cells as detected by nuclear staining (DAPI). Tumor borders are defined by the increased density of nuclei.

A.

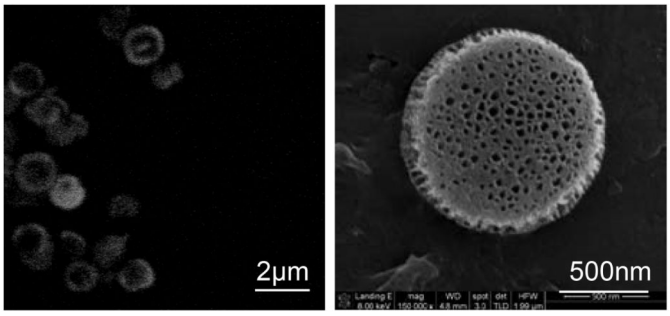

B.

Zeta potential of MSV(APTES)	8.95±0.23
Zeta potential of MSV-BSA-FITC	-23.02±1.47
Zeta potential of MSV-nAb-PTX	-16.6±0.85
MSV-FITC-BSA loading efficiency	78-94%
MSV-nAb-PTX loading efficiency	35-64%

C.

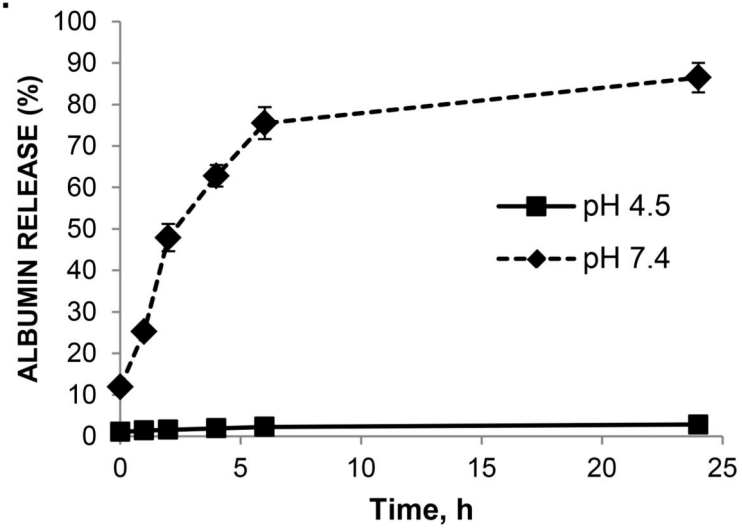

Figure 2. Loading and release of nAb-PTX in MSV

(A) Confocal microscopic images of MSV loaded with a fluorescent probe bound to albumin (FITC-albumin) (left) and scanning electron microscopy image of MSV loaded with MSV-nAb-PTX (right); (B) Changes in zeta potential of MSV as a result of loading with FITC-albumin and nAb-PTX and loading efficiency of these molecules; (C) Release of FITC-albumin from MSV in PBS (pH 7.4) and acetic buffer (pH 4.5).

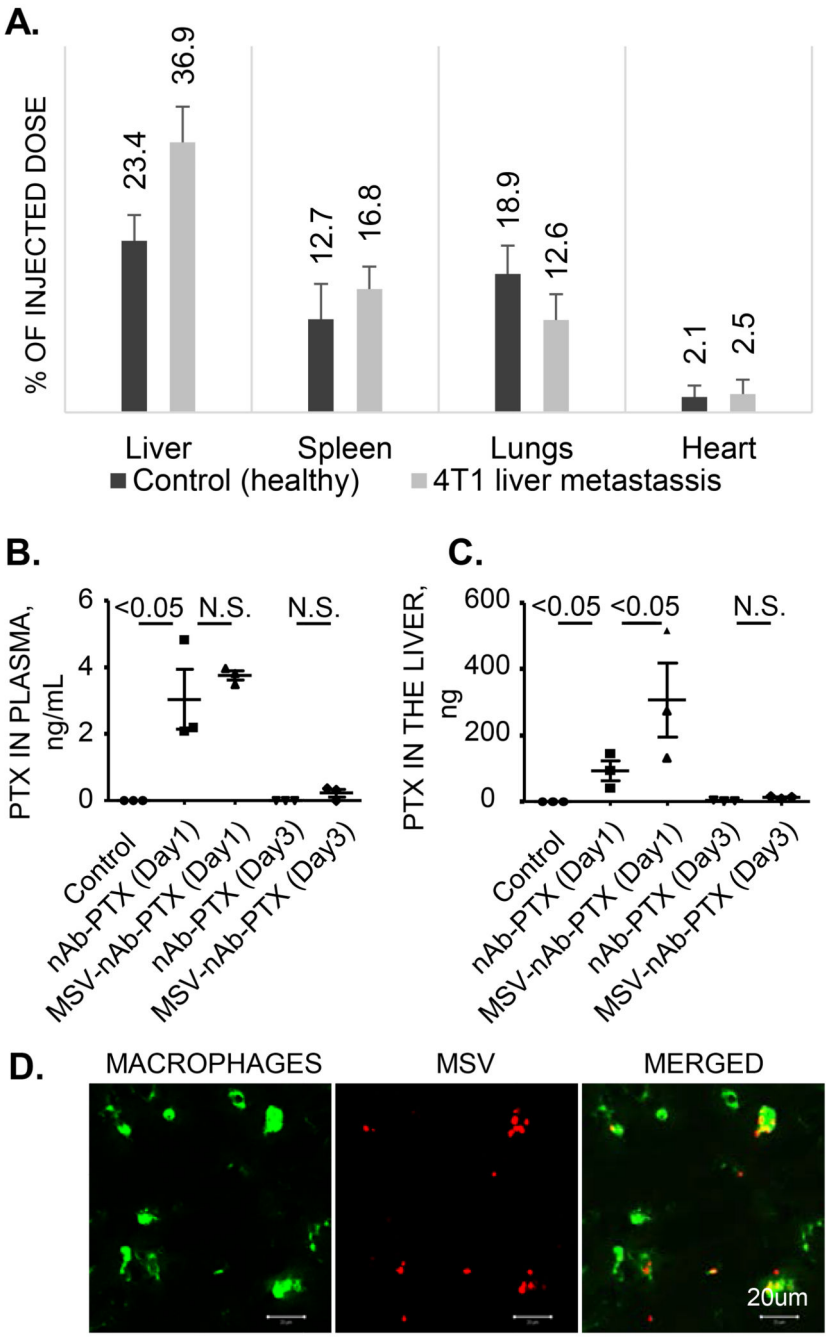

Figure 3. Biodistribution of MSV-nAb-PTX

(A) Organ distribution of MSV injected in healthy mice and mice bearing breast cancer (4T1) lesions in the liver as determined by the elemental analysis of silicon using Inductive couples plasma atomic emission spectroscopy (ICP-AES); Levels of PTX in plasma (B) and in the liver (C), 1 and 3 days after intravenous injection of MSV-nAb-PTX and nAb-PTX into the tumor bearing mice; (D) Association of intravenously injected fluorescently labeled MSV (red) with liver macrophages (green).

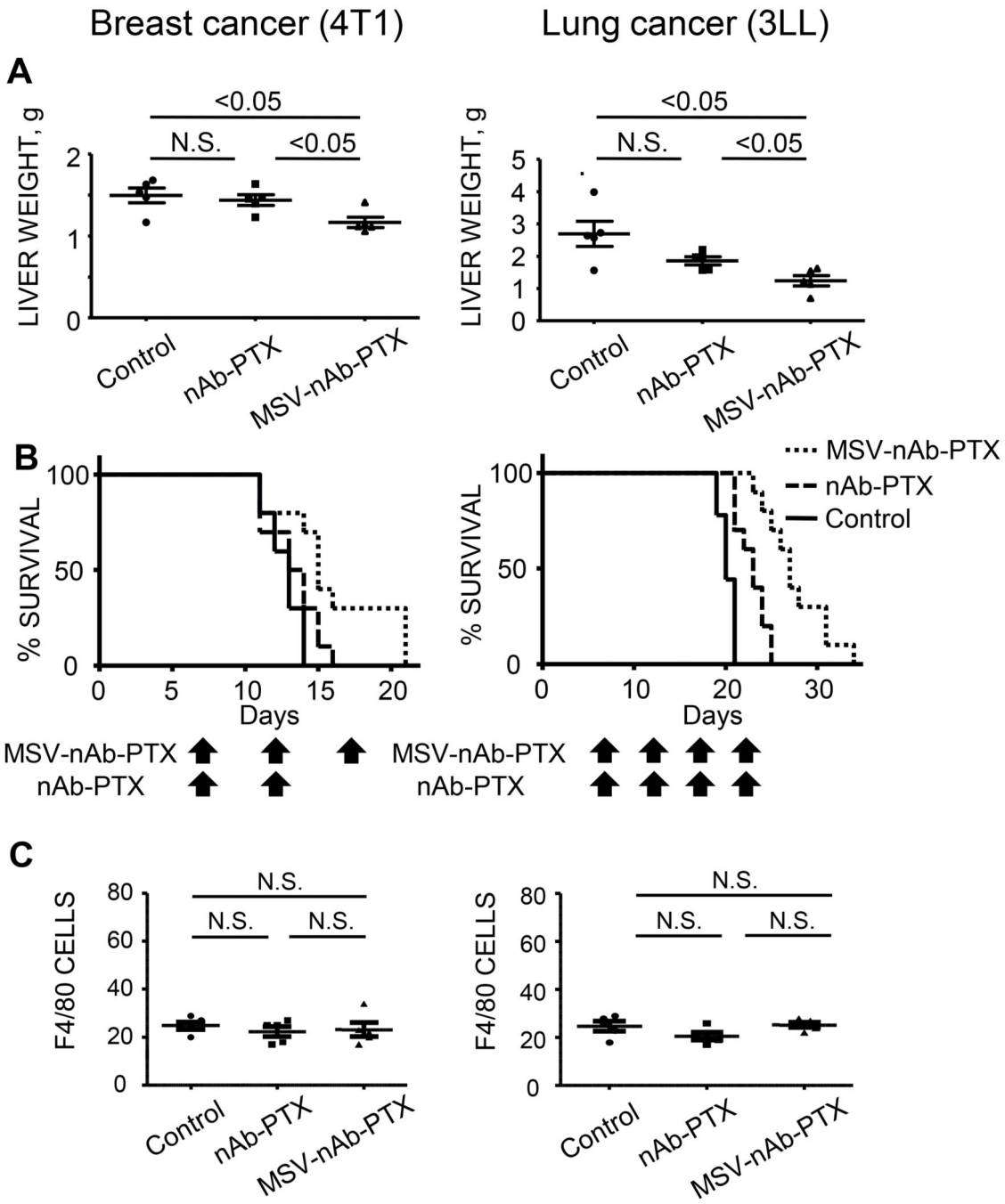

Figure 4. Therapeutic efficacy and survival of mice bearing breast (left) and lung (right) cancer liver metastasis following intravenous administration of MSV-nAb-PTX, or nAb-PTX

(A) Liver weight as a parameter of tumor burden. MSV-nAb-PTX treatment caused significant inhibition in development of 4T1 breast and 3LL lung cancer liver metastases as compared to nAb-PTX ($P<0.05$ in both models). (B) Kaplan-Meier curves for survival of mice. Mice were injected intrasplenically with cancer cells and the therapy was initiated one week later. The therapy was administered every 5 days until the animals are moribund. (Log-rank test for MSV-nAb-PTX vs. nAb-PTX is $P<0.05$ for 4T1 and $P<0.01$ for 3LL

models, respectively). (C) The effect of nAb-PTX and MSV-nAb-PTX on the number of macrophages (F4/80) / field of view in the unaffected liver.

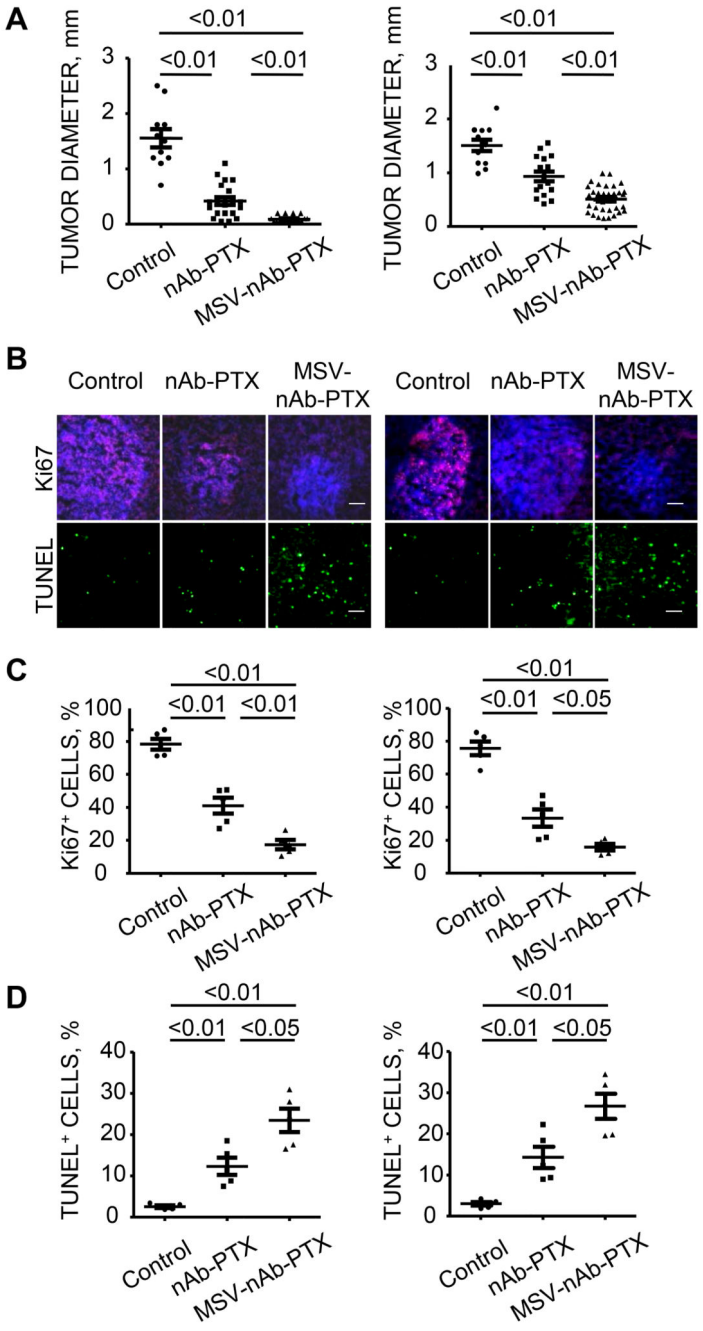

Figure 5. Histological and immunofluorescent analysis of MSV-nAb-PTX and nAb-PTX effects on the breast (left) and lung (right) liver metastasis

(A) quantification of the tumor diameters in the liver of the mice treated with control, nAb-PTX or MSV-nAb-PTX (MSV-nAb-PTX vs. nAb-PTX, P <0.01 in both models); Immunohistochemical staining (B, scale bar 100μm) and quantitative analysis (C, D) of proliferating Ki67-positive cancer cells (pink) and apoptotic TUNEL-positive cancer cells (green). Nuclei were stained with DAPI (blue).

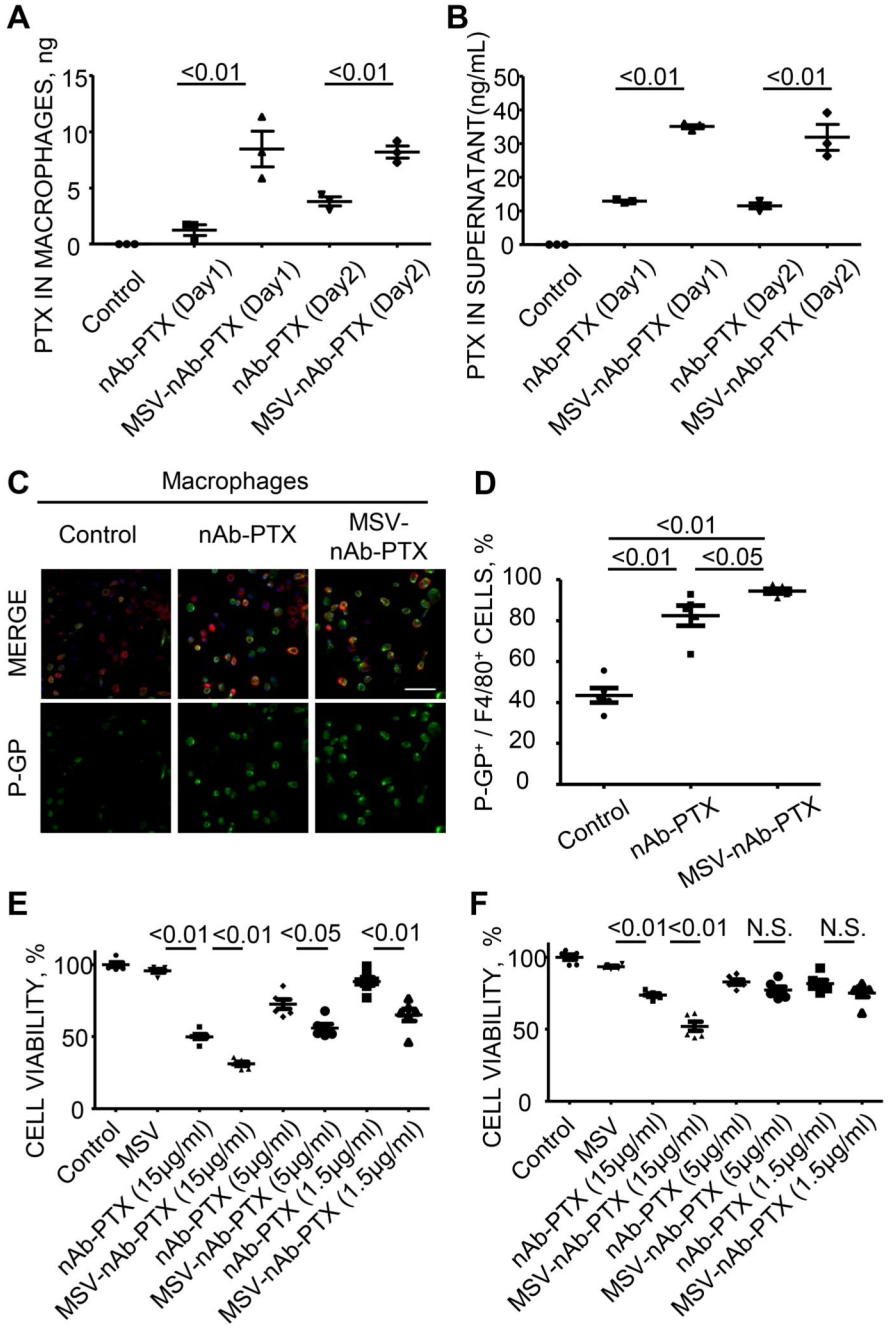

Figure 6. Macrophages as depot for MSV-nAb-PTX

(A) Retention of PTX in macrophages ; (B) the release of PTX to the cell culture medium following incubation of the cells with MSV-nAb-PTX or nAb-PTX; (C) Immunofluorescence imaging; and (D) quantification of the expression of p-glycoprotein efflux pumps (green) in macrophages (red) treated with control PBS, nAb-PTX or MSV-nAb-PTX (scale=100μm); Cytotoxic effect of released PTX from macrophages pre-

incubated with control PBS, empty MSV, different dose of nAb-PTX or MSV-nAb-PTX on cancer cells evaluated by MTT assay (E: 4T1 cells, F: 3LL cells).